Multiscale regulation of S, N, O tri-doped carbon/Co_8FeS_8 catalysts with SO_4^{2-}-riched and lattice distortion for efficient water splitting

Yuanrong Ye[a], Xin Zhao[a]*, Guijuan Wei[a]*, Shaonan Gu[a], Changwei Li[a], Huixin Zhang[a], Junliu Zhang[a], Xiaoyang Li[a], Honglei Chen[a]*

[a]State Key Laboratory of Biobased Material and Green Papermaking, Qilu University of Technology, Shandong Academy of Sciences, Jinan 250353, P.R. China

*Corresponding author: Xin Zhao, Guijuan Wei, Honglei Chen. Tel/Fax: +86-0531-89631168.

E-mail: zhaoxin_zixi@126.com (Xin Zhao), weiguijuan@qlu.edu.cn (Guijuan Wei), chenhonglei_1982@163.com (Honglei Chen)

Characterization

A scanning electron microscope (SEM, Regulus 8220, Japan) was used to examine the surface morphologies and elemental composition of materials. An FEI Tecnai G2 F20 transmission electron microscopy (TEM) apparatus with a 200-kV voltage was used to characterize the morphology. The crystal structure of the samples was studied by X-ray diffractometer (Germany, Cu K radiation). The valence and chemical states of the surface elements of the samples were determined by X-ray photoelectron spectroscopy (XPS, Escalab 250 Xi, USA). Raman spectra of the samples were acquired using a LabRAM Hr800 confocal Raman microscopic system and a 532 nm excitation laser. The uncoordinated electrons of the samples were tested using an electron paramagnetic resonance (EPR)spectrometer (Bruker EMXplus).

Electrochemical Tests and Calculations

Thorough assessment of the materials' electrocatalytic performance for OER and HER was carried out using a typical three-electrode arrangement with the electrochemical workstation CHI 660E. Ag/AgCl (saturated KCl solution) and carbon rod were used as reference and counter electrodes. The working electrodes were prepared as follows：the samples were ground into a powder using a mortar. Afterward, the sample was dispersed in 460 μL of water/ethanol mixed solvents (300 μL of ethanol, 160 μL water) along with 40 μL of Nafion solution (5 wt%), and the mixture was sonicated for about 30 min to generate a homogeneous catalyst ink. Then, 50 μL of the above solution was drop-cast onto the NF and dried at room temperature, leading to a catalyst loading of 2.5 mg cm^{-2}. The electrolyte solution was 1 M KOH solution. The geometric area of NF is used to standardize the current density. The recorded potential is converted to a reversible hydrogen electrode scale :

$$E(RHE) = E(Ag/AgCl) + 0.197 + 0.059 \times pH,$$

Linear sweep voltammetry (LSV) polarization curves were obtained using ohmic potential drop (iR) correction in 1 mol KOH solution at a scan rate of 10 mV s^{-1}. The cyclic voltammetry curves were examined at seven different scan rates (10, 20, 40, 60, 80, 100and 120 mV s^{-1}) within a voltage range of 0-0.1 V, and the corresponding current density values were obtained. The double-layer capacitance (C_{dl}) and of the samples were obtained at different scan rates using $\Delta j\ (ja - jc)/2$. The electrochemically active surface area (ECSA) was determined by normalizing the double-layer capacitance (C_{dl}) to the specific capacitance of 0.04 mF cm^{-2}. Specific activity was calculated using the following equations:

$$\text{Specific activity} = \frac{j * A}{ECSA}$$

where j is the current density; A is the surface area, and ECSA is the electrochemical surface area.

Using chronoamperometry (i-t) at a fixed voltage to evaluate the durability of the sample. The overall water splitting performance of the samples was tested in a two-electrode mode.

Fig. S1 Precursor of SNO-C/Co_8FeS_8

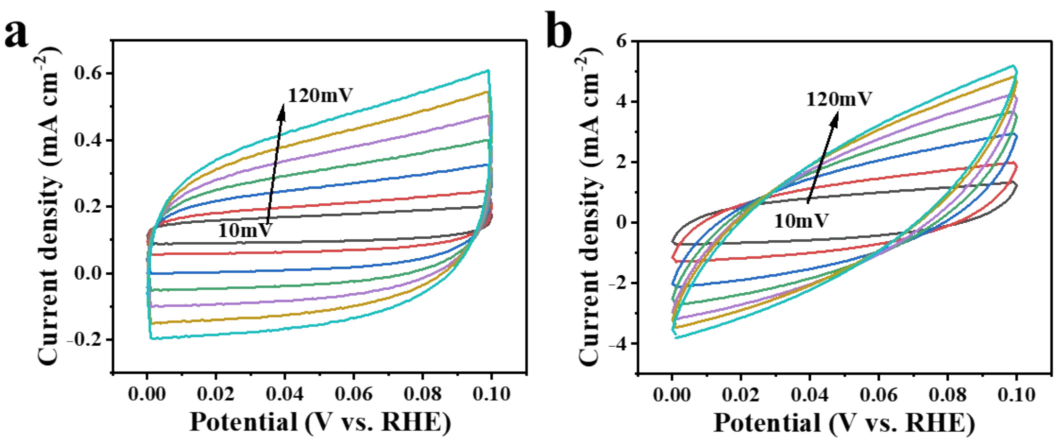

Fig. S2 CV curves of SN-Co_8FeS_8 and SNO-C/Co_8FeS_8 at different scanning rates.

Table S1. Comparison of OER performance in 1 M KOH solution for SNO-C/Co_8FeS_8 with other metal electrocatalysts.

Catalyst	Overpotential @j mA cm^{-2} (mV @ j)	Reference
SNO-C/Co_8FeS_8	230@10 268@100 290@400	This work
CFS-ACs/CNT	270@20	Nature Communications (2024) 15:1720
Fe−Ni−Co-MOF	236@10	ACS Catal. 2024, 14, 1553−1566
$(NiFeCoMn)_3S_4$	289@10	Adv. Funt. Mater. 2023, 33, 2208170.
$(CrMnFeCoNi)S_x$	295@100	Adv. Energy Mater. 2021, 11, 2002887.
Ni-Fe-S/NCQDs	295@10	Appl. Catal. B-Environ. 2023, 324, 122230.
CoS_2/MoS_2	255@10	Chem. Eng. J. 2023, 470, 144372.
NiFe alloy	298@10	Catalysis Today, 2020, 352: 27-33
$Fe_2O_3/Fe_{0.64}Ni_{0.36}$@C-800	274@10	Small 2023, 2208276
Fe-NiS_2/NCNT	292@10	J. Colloid Interf. Sci. 581 (2021) 608 – 618

Table S2. Comparison of HER performance in 1 M KOH solution for SNO-C/Co_8FeS_8 with other metal electrocatalysts.

Catalyst	Overpotential @j mA cm^{-2} (mV @ j)	Reference
SNO-C/Co_8FeS_8	120@10 235@100 365@400	This work
Co@NPC-800	274@10	Chemical Engineering Journal 430 (2022) 132783
Mo-Ni_3S_4/CW-0.4	240@10 337@100	Applied Catalysis B: Environmental 339 (2023) 123123
Co_8FeS_8@CoFe– MOF/NF	361@10 473@100	Journal of Colloid and Interface Science 634 (2023) 630–641
Co_9S_8	295@100	Small 2022, 18, 2204309
$Co_{0.25}Fe_{0.75}$-LDH	365@10	ACS Catal. 2023, 13, 1477−1491
Co@NCNT/CW	209@100	Adv. Energy Mater. 2023, 2300427
Co-ALMO@NF	302@100 349@500	Adv. Sci. 2023, 10, 2206952
Ni2P/FeP-FF	207@100	Adv. Funct. Mater. 2023, 33, 2302621
$Co_2N_{0.67}$-BHPC	210@10	Journal of Energy Chemistry 54 (2021) 626–638

Table S3. Electrochemical results of the catalysts.

Samples	C_{dl} (mF cm^{-2})	ECSA (cm^2)	Specific activity (mA cm^{-2}) @ 1.52 V	J (mA cm^{-2}) @ 1.52 V
SNO-C/Co_8FeS_8	23.09	577.25	0.6929	400
SN-Co_8FeS_8	0.47	11.75	0.6136	7.21

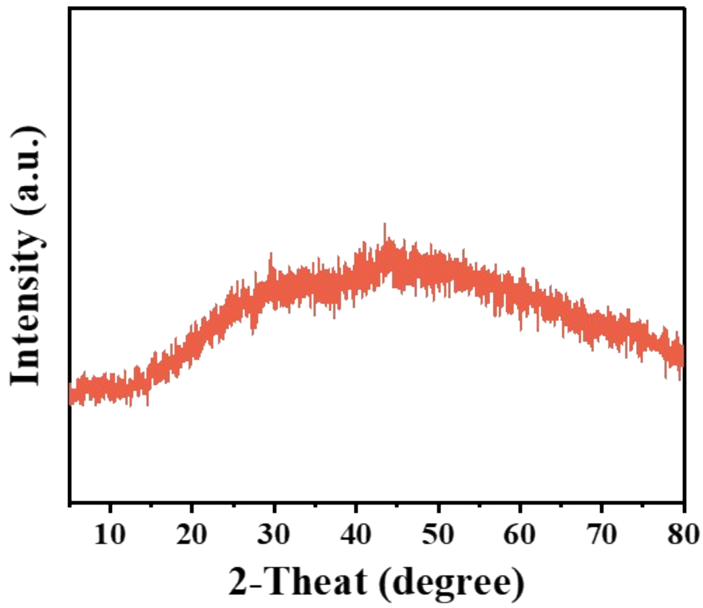

Fig. S3 XRD pattern after 50 h i-t test at OER process.

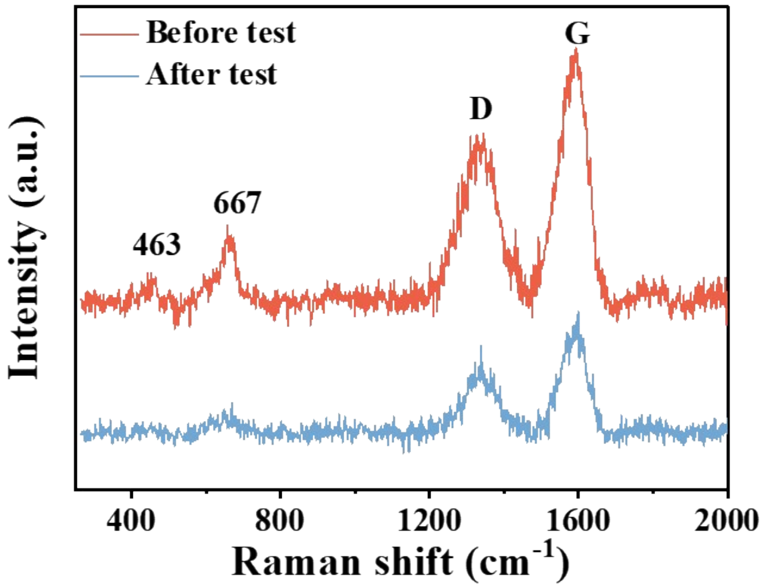

Fig. S4 Raman spectra after 50 h i-t test at OER process.

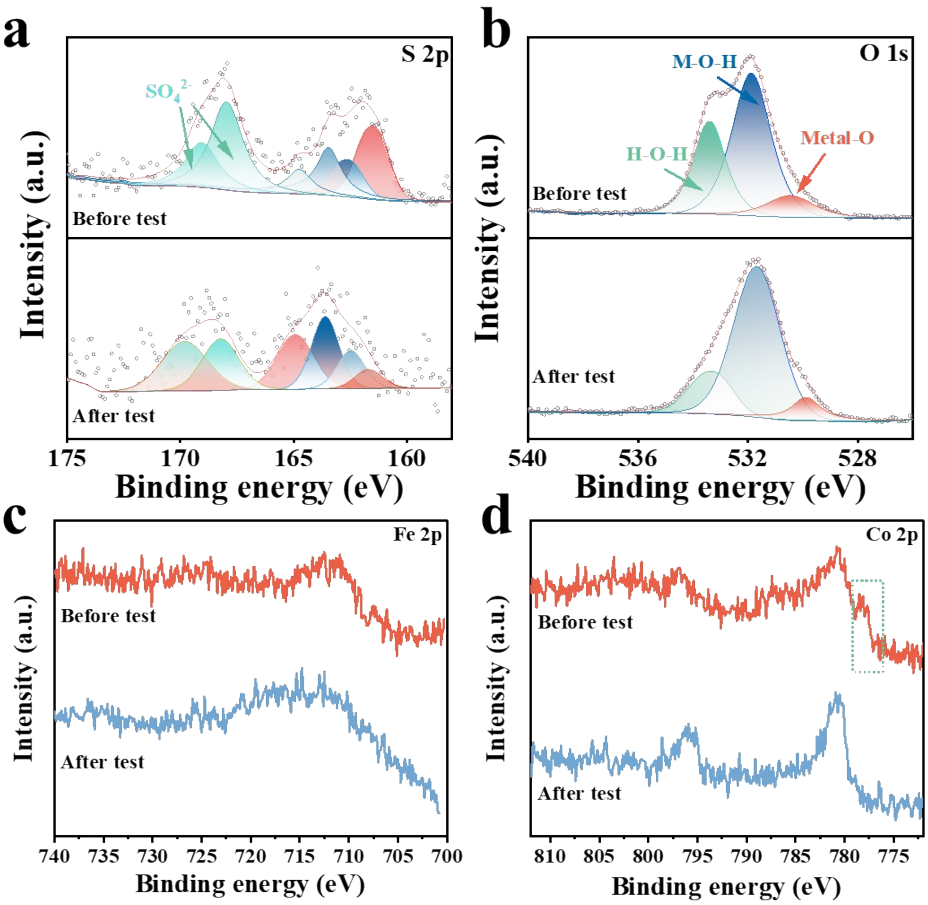

Fig. S5 High resolution XPS survey spectra of (a) S 2p, (b) O 1s, (e) Fe 2p and (f) Co 2p spectra after 50 h i-t test at OER process.

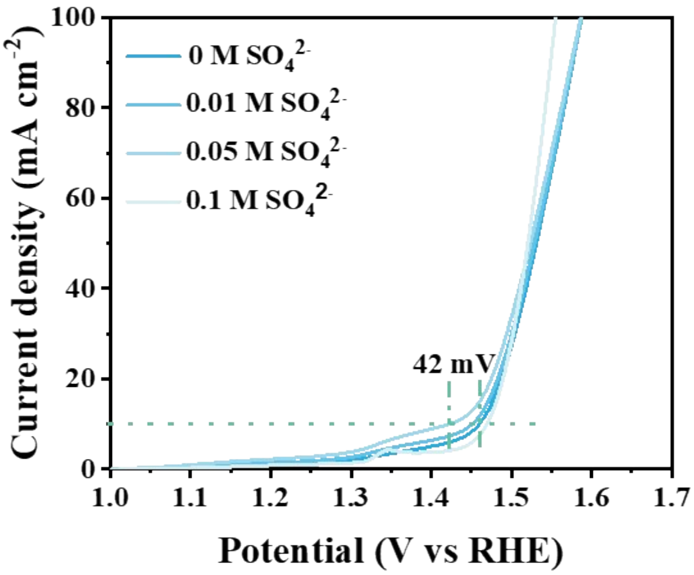

Fig. S6 LSV curves of SNO-C/Co_8FeS_8 tested in 1 M KOH electrolyte supplemented with different concentrations of SO_4^{2-}.

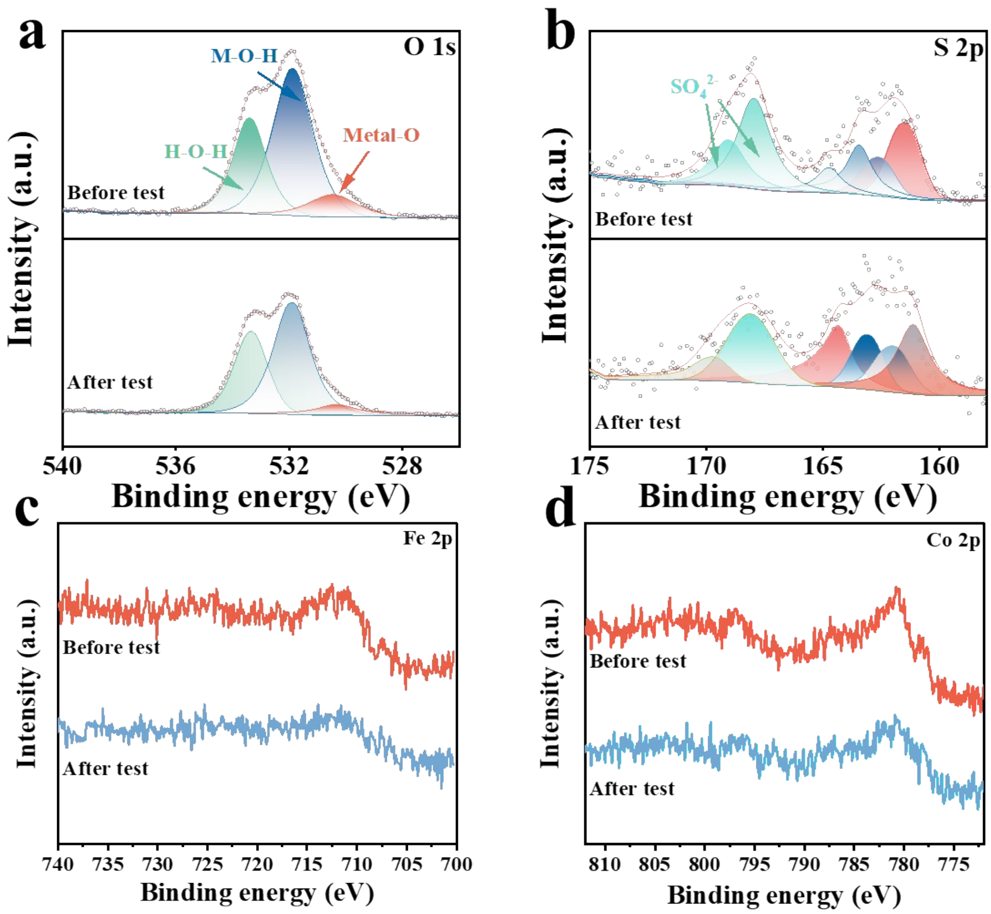

Fig. S7 High resolution XPS survey spectra of (a) S 2p, (b) O 1s, (e) Fe 2p and (f) Co 2p spectra after 50 h i-t test at HER process.

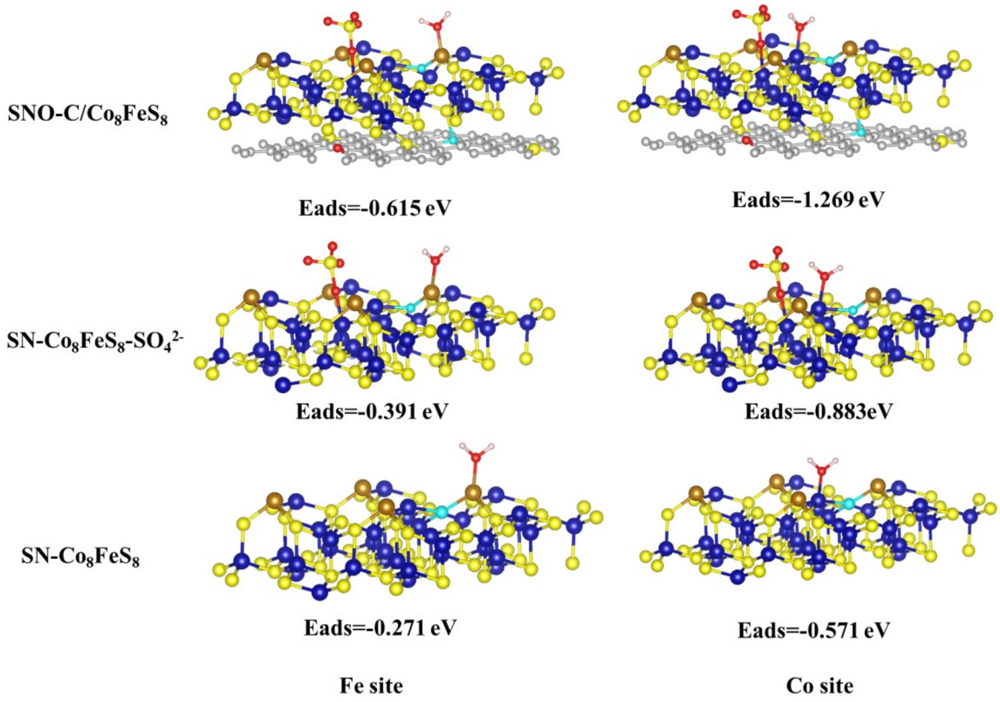

Fig. S8 The adsorption models of SNO-C/Co_8FeS_8, SN-Co_8FeS_8-SO_4^{2-} and SN-Co_8FeS_8 on Fe and Co sites for H_2O.

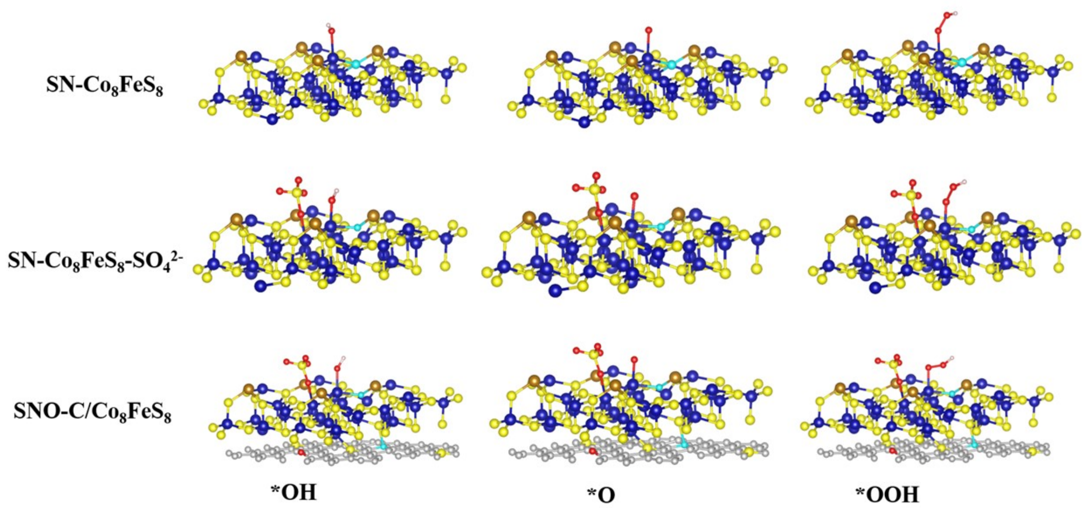

Fig. S9 Adsorbed structures of *O, *OH and *OOH of OER.

Theoretical calculation Methods

We have employed the first-principles [1,2] to perform density functional theory (DFT) calculations within the generalized gradient approximation (GGA) using the Perdew-Burke-Ernzerhof (PBE) [3] formulation. We have chosen the projected augmented wave (PAW) potentials [4,5] to describe the ionic cores and take valence electrons into account using a plane wave basis set with a kinetic energy cutoff of 500 eV. The GGA+U method was adopted in our calculations. The value of the effective Hubbard U was set as 4.931 eV for Co Partial occupancies of the Kohn−Sham orbitals were allowed using the Gaussian smearing method and a width of 0.1 eV. The electronic energy was considered self-consistent when the energy change was smaller than 10^{-5} eV. A geometry optimization was considered convergent when the energy change was smaller than 0.05 eV $Å^{-1}$. The Brillouin zone integration is performed using 2×2×1 Monkhorst-Pack k-point sampling for a structure. Finally, the adsorption energies(Eads) were calculated as Eads= Ead/sub -Ead -Esub, where Ead/sub, Ead, and Esub are the total energies of the optimized adsorbate/substrate system, the adsorbate in the structure, and the clean substrate, respectively. The free energy was calculated using the equation:

G=Eads+ZPE-TS

where G, Eads, ZPE and TS are the free energy, total energy from DFT calculations, zero point energy and entropic contributions, respectively, where T is set to 300K.

The d-band center Spin up/down was calculated by the following formula:

$$d_{up/down} = \frac{\int_{-\infty}^{\infty} \varepsilon_d(\varepsilon)\varepsilon dx}{\int_{-\infty}^{\infty} \varepsilon_d(\varepsilon) dx}$$

where ε is the energy level and $\varepsilon_d(\varepsilon)$ is DOS.

The finally d-band center $= \frac{d_{up} + d_{down}}{2}$.

References

1. Kresse, G.; Furthmüller, J. Efficiency of Ab-Initio Total Energy Calculations for Metals and Semiconductors Using a Plane-Wave Basis Set. Comput. Mater. Sci. 1996, 6, 15−50.

2. Kresse, G.; Furthmüller, J. Efficient Iterative Schemes for Ab Initio Total-Energy Calculations Using a Plane-Wave Basis Set. Phys. Rev. B 1996, 54, 11169−11186.

3. Perdew, J. P.; Burke, K.; Ernzerhof, M. Generalized Gradient Approximation Made Simple. Phys. Rev. Lett. 1996, 77, 3865−3868.

4. Kresse, G.; Joubert, D. From Ultrasoft Pseudopotentials to the Projector Augmented-Wave Method. Phys. Rev. B 1999, 59, 1758-1775.

5. Blöchl, P. E. Projector Augmented-Wave Method. Phys. Rev. B 1994, 50,

17953−17979.
6. V. Wang, N. Xu, J.C. Liu, G. Tang, W.T. Geng, VASPKIT: A User-Friendly Interface Facilitating High-Throughput Computing and Analysis Using VASP Code, Computer Physics Communications 267, 108033 (2021)